High-accuracy sinusoidal phase-modulating self-mixing interferometer using an electro-optic modulator: development and evaluation

Wei Xia, Ming Wang,* Zhenyu Yang, Wenhua Guo, Hui Hao, and Dongmei Guo

Jiangsu Key Laboratory on Opto-electronic Technology, Department of Physics Science and Technology, Nanjing Normal University, Nanjing 210046, China

*Corresponding author: wangming@njnu.edu.cn

Received 25 June 2012; revised 1 November 2012; accepted 20 December 2012; posted 2 January 2013 (Doc. ID 171025); published 21 January 2013

A sinusoidal phase-modulating He–Ne laser subject to weak optical feedback has been used to develop an interferometer that is capable of performing real-time displacement measurement with nanometer accuracy. The principle and the signal processing method are introduced. A commercial dual-frequency interferometer is included in the displacement measurement in both small and large ranges to evaluate the performance of the developed interferometer. Experimental results show that the average errors and standard deviations of the interferometer are in good agreement with data obtained from the commercial interferometer. The resolution and the multiple feedback effect of the interferometer are discussed in detail. These results show that the development of the interferometer is reasonable and feasible. © 2013 Optical Society of America

OCIS codes: 120.3180, 120.5050, 120.5060.

1. Introduction

In recent decades, with the steadily increasing importance of microelectromechanical systems and nanostructures in different technology fields, it becomes more crucial to measure large displacements of mechanical components with the high accuracy of a few nanometers [1–3]. Typically, there are two kinds of approaches in conventional nanometrology. One is the nonoptical methods, and examples are the scanning tunneling microscope (STM) and atomic force microscope (AFM). The other is the optical measurement techniques, including the Michelson interferometer, Fabry–Perot interferometer, heterodyne interferometer, etc. Although ultrahigh-resolution microscopic techniques like STM and AFM are widely used today, optical methods are still of great interest and importance because they are fast, contamination free, and nondestructive and have good in-line capability [4].

Both heterodyne and homodyne interferometers have been comprehensively used for precision measurements of large displacements [5,6]. Such large displacement measurement can also be carried out using a Michelson interferometer with multiple measurement wavelengths or the frequency shifting technique [7–9]. However, a major drawback of these existing methods is the high complexity of system construction, which increases system cost. Compared with these well-established interferometers, the self-mixing interferometer (SMI) is characterized by its capability of high performance with an extremely simple and inexpensive experimental setup and its potential in direct industrial applications for vibration and displacement sensing [10,11]. Among different kinds of optical techniques based on SMI applied for these displacement measurements, the

1559-128X/13/040B52-08$15.00/0

sinusoidal phase-modulating interferometer is the most competitive due to the benefit of time-continuous operation, easy implementation, high accuracy, and immunity to optical and electronic noises [12–14]. A sinusoidal phase-modulating interferometer based on a laser diode (LD) has been reported to perform displacement measurement with high accuracy [15]. However, the disadvantage of injection current modulation is the unwanted intensity modulation concurrent with the wavelength modulation, which results in measurement errors. Several methods have been developed to weaken the influence of the intensity modulation of LDs, and this effect can be greatly reduced [16,17]. Instead of designing a new signal processing algorithm, an electro-optic modulator (EOM) was used to generate pure phase shifting in an optical feedback interferometer, where the intensity modulation effect can be entirely avoided [18,19]. Nonetheless, both the modulation and demodulation techniques of these displacement sensors were carried out in the time domain, and the phase of the interference signal was retrieved from several adjacent sampled data. It is preferable to process the interference signal in the frequency domain, where complete information of the interference signal is maintained and the sensitivity of the system to noises has been reduced. Moreover, the measurement accuracy can be further improved.

The main objective of this paper is to develop a sinusoidal phase-modulating SMI for industrial applications that is able to realize large displacement measurement with nanometer resolution. The paper is organized as follows. Section 2 demonstrates the model of the sinusoidal phase-modulating SMI and its operation principle. Section 3 will provide the signal processing technique. In Section 4, displacement measurement experiments and a comparison between our system and an Agilent 5529A interferometer are described, while in Section 5, the resolution and the multiple feedback effect of the SMI are discussed in detail.

2. Measurement Principle

The schematic diagram of the sinusoidal phase-modulating SMI is illustrated in Fig. 1. The linearly polarized light beam emitted by a He–Ne laser propagated through a various neutral density (ND) filter and an EOM and then reflected back to the laser cavity by a movable object, forming the self-mixing effect. Therefore, laser operations are altered and the self-mixing interference signal is monitored by a photodiode (PD) placed behind the back mirror of the laser. The polarization of the laser is set parallel to the electro-optically active axis of the EOM, so that a pure phase modulation is obtained. The object is fixed on a commercial piezoelectric transducer (PZT). When the signal processing unit sends a signal to the PZT controller, the object is moved a measured displacement ΔL. The output signal of the PD is fed into the signal processing unit to retrieve the measured displacement in real time.

Assuming that SMI operates in a low-feedback regime where the effect of multiple reflections in the external cavity is small, the interference signal detected by the PD with sinusoidal phase modulation $\psi(t)$ is given by [15]

$$I(t) = I_0\{1 + m\cos[\varphi(t) + \psi(t)]\} \tag{1}$$

with

$$\varphi(t) = 4\pi nL(t)/\lambda_0, \tag{2}$$

where I_0 denotes the unperturbed optical output power. $\varphi(t)$ is the measured phase of the external cavity, m is the fringe visibility, n is the refractive index of air, $L(t)$ is the length of the external cavity, and λ_0 is the central wavelength in vacuum. $\psi(t) = 2a\sin(w_M t + \beta)$ is the sinusoidal phase modulation term. Considering that the light beam passes through the EOM twice in the external cavity, the sinusoidal phase modulation depth is $2a$. The frequency and initial phase are w_M and β, respectively. Expanding Eq. (1), we obtain

$$\begin{aligned} I(t) = I_0[1 &+ m\cos\varphi(t)J_0(2a)] \\ &+ 2mI_0\cos\varphi(t)\sum_{n=1}^{\infty}J_{2n}(2a)\cos(2n)(w_M t + \beta) \\ &- 2mI_0\sin\varphi(t)\sum_{n=1}^{\infty}J_{2n-1}(2a) \\ &\times\cos[(2n-1)(w_M t + \beta)], \end{aligned} \tag{3}$$

where $J_{2n-1}(2a)$ and $J_{2n}(2a)$ denote the odd- and even-order Bessel functions, respectively. Inspection of Eq. (3) shows that the ac component of the SMI signal is composed of the fundamental frequency w_m and its harmonics. The odd harmonics vary as $\sin[\varphi(t)]$, and the even harmonics vary as $\cos[\varphi(t)]$. And then the measured phase $\varphi(t)$ can be figured out from comparing the intensities of these frequency components. Considering that the strength of the nth-order harmonic component is proportional to the value of nth-order Bessel function, which becomes progressively smaller with the increment of the order, only the lowest few harmonics are important, and the phase $\varphi(t)$ is therefore obtained using the following equation:

$$\varphi(t) = \arctan\left[\frac{J_2(2a)}{J_1(2a)}\cdot\frac{A_1(t)}{A_2(t)}\right], \tag{4}$$

where $A_1(t)$ and $A_2(t)$ denote the intensities of first and second harmonics, respectively. The phase information $\varphi(t)$ in Eq. (4) is wrapped into the interval of $(-\pi, +\pi)$, and an unwrap process is required to get a continuous value of $\varphi(t)$.

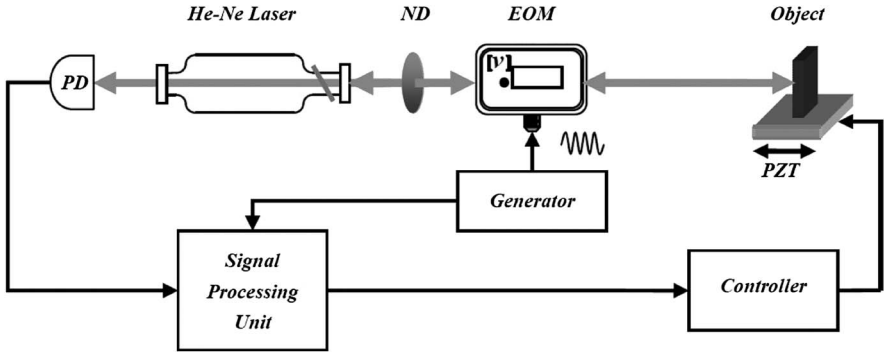

Fig. 1. Schematic diagram of the sinusoidal phase-modulating SMI.

3. Signal Processing

According to the above description, the signal processing of a sinusoidal phase-modulating SMI includes the optical part and the electronic design.

A. Self-Mixing Interference Signal Processing

Figure 2(a) shows a simulated sinusoidal phase-modulating SMI signal received by a PD when the object moves sinusoidally. The Fourier spectra of the SMI signal illustrated in Fig. 2(b) conforms to Eq. (3), so that it is convenient to obtain the first and second harmonics by two filters in the frequency domain. After removal of the carrier, the upper curve $A_1(t)$ in Fig. 2(c) signifying the intensity of the first harmonic is obtained. The lower curve $A_2(t)$ signifying the intensity of the second harmonic is obtained in a similar way. The curves $A_1(t)$ and $A_2(t)$ are used to determine the wrapped measured phase between $-\pi$ and $+\pi$ shown in Fig. 2(d). In addition, an unwrapping process is needed to reconstruct a continuous phase variation of the SMI signal.

B. Implementation of Signal Processing

The real-time signal processing unit of a sinusoidal phase-modulating SMI is demonstrated in Fig. 3. An application program in laboratory virtual engineering workbench (LabVIEW) is used for the realization of data processing. The SMI signal monitored by the PD is filtered, amplified, and converted to digital signals for subsequent processing. First, the fast Fourier transform of the digitalized interference signal is taken, and the frequency content is fed to two bandpass filters to select the first and second harmonics separately. Second, the inverse fast Fourier transform of the filtered components is performed, and the intensities of the first and second harmonics are obtained by removing the carriers. Third, the phase determination unit calculated the wrapped phase of the interference signal within the range of $(-\pi, \pi)$ by using Eq. (4). After a phase unwrapping process, the measured phase of an object can be retrieved.

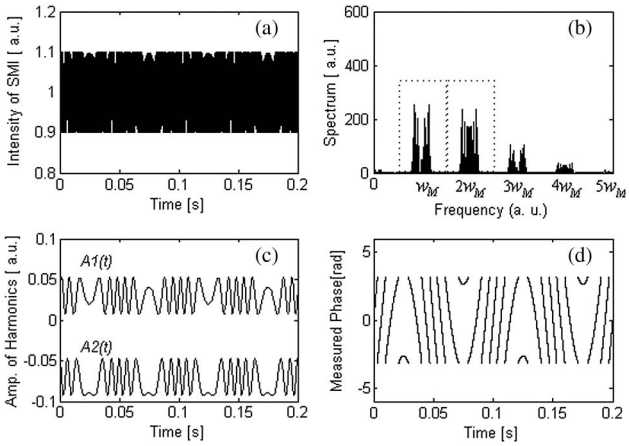

Fig. 2. Realization of interference signal processing: (a) simulated phase modulating SMI signal, (b) frequency spectrum of SMI signal, (c) intensities of the first and second harmonics, and (d) wrapped measured phase.

4. Experimental Results

To evaluate its performance, the sinusoidal phase-modulating SMI with the calibration part was developed as shown in Fig. 4. The laser source was a He–Ne laser (1 mW), which emits a vertically polarized beam with a central wavelength of 632.8 nm. A various ND filter is used to assure that the SMI operates in a low-feedback regime, and sinusoidal phase modulation is introduced by EOM (New Focus, 4002). The measured displacement of the object is provided by a linear stage whose movement range is 300 mm with 1 μm resolution and a nanopositioning stage (P-762.2L, Physik Instrumet Co., Germany) whose movement range is 100 μm with 1 nm resolution. A commercial heterodyne interferometer (5529A, Agilent Co., USA) with 1 nm resolution was used to test the displacement of the same object for comparison. As for practical use, the optical part of our system only consists of a PD, a He–Ne laser, an ND filter, and an EOM. We can see that the developed interferometer includes a simple, single-axis optical arrangement that requires minimal optical components.

When the object was moved a measured displacement ΔL, the phase-modulated SMI signal was sent to the signal processing unit for calculating the displacement. Meanwhile, the same movement was recorded by an Agilent interferometer. Experiments were carried out in the millimeter range, micrometer range, and nanometer range.

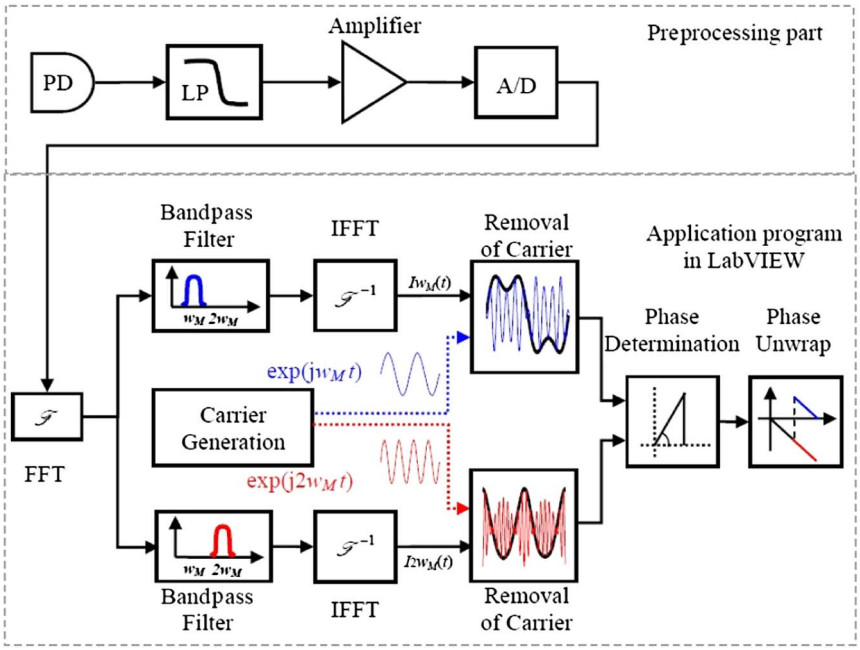

Fig. 3. (Color online) Schematic diagram of the signal processing of a sinusoidal phase-modulating SMI. LP, low-pass filter; FFT, fast Fourier transform; IFFT, inverse fast Fourier transform.

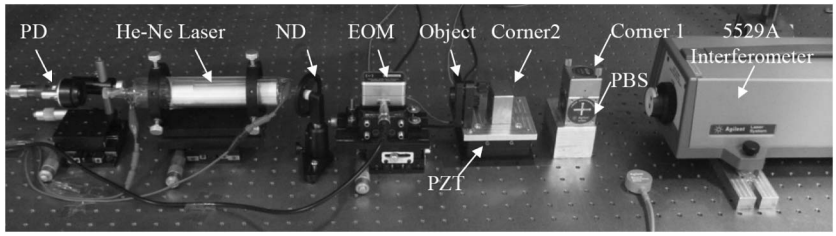

Fig. 4. Photo of experimental setup. PBS, polarized beam splitter.

A. Displacement Measurement Experiment in the Millimeter Range

In this experiment, displacements of the object were performed by moving the linear stage with a sampling interval of 5 mm within the range of 100 mm. The velocity of the object was set to 2.5 mm/s, so that the average time for each of the measurements was about 2 s. These displacements were measured simultaneously by the SMI and the Agilent interferometer. The experimental result is shown in Fig. 5 and summarized in Table 1. The deviations denote the differences between the actual displacements of the linear stage and the measurement results with the SMI or with the Agilent interferometer. The linearity coefficient can be obtained by linear fitting and is shown in Table 1. Figure 5 and Table 1 show that the results with our system are in good agreement with data obtained with the Agilent interferometer. These results demonstrate that our system can be applied to displacement measurement in the millimeter range.

B. Displacement Measurement Experiment in the Micrometer Range

In this experiment, displacements of the object were performed by moving the nanopositioning stage for a traveling range of 100 μm, which is divided into 20 steps with a step size of 5 μm. The velocity of the object was set to 50 μm/s, so that the maximum measurement time was about 2 s. The experimental result is shown in Fig. 6 and summarized in Table 2, showing that the results with our system are in good

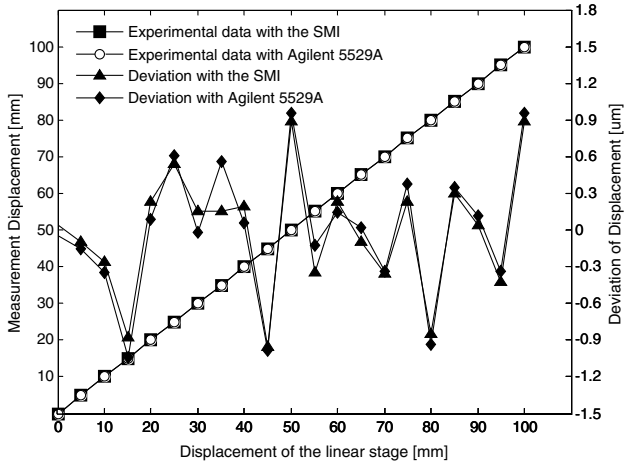

Fig. 5. Comparison of displacement measurements in the millimeter range.

Table 1. Displacement Measurement Results in the Millimeter Range

System	Averaged Error (μm)	Standard Deviation (μm)	Maximum Error (μm)	Linearity Coefficient
The SMI	−0.0169	0.5061	0.9558	0.9998
Agilent 5529A	−0.0057	0.5535	1.0424	0.9998

accordance with data obtained by the Agilent interferometer. These results demonstrated that the SMI can be applied to micrometer-range displacement measurement with nanometer accuracy.

C. Displacement Measurement Experiment in the Nanometer Range

In this experiment, the object was moved for a travel distance of 500 nm, with a sampling interval of 25 nm. The velocity of the object was set to 250 nm/s, so that the maximum measurement time was about 2 s. The experimental results with the SMI and 5529A interferometer and the deviations compared with the nanopositioning stage's displacement are shown in Fig. 7 and summarized in Table 3. This shows that the results with SMI are in good agreement with data from the Agilent interferometer. These results further demonstrate that the sinusoidal phase-modulating SMI can achieve nanometer-level accuracy.

D. Displacement Measurement Experiment with Sinusoidal or Saw-Wave Form

We conducted further experiments, in which the object was mounted on the nanopositioning stage and moved in a saw-wave or sinusoidal form with several different amplitudes from about 20 μm down to 100 nm. The measurement results by our system are shown in Fig. 8, and the measured displacement amplitude by the SMI and Agilent interferometer are summarized in Table 4. From these results, it can be concluded that our system was able to perform sinusoidal or saw-wave displacement measurement with nanometer accuracy.

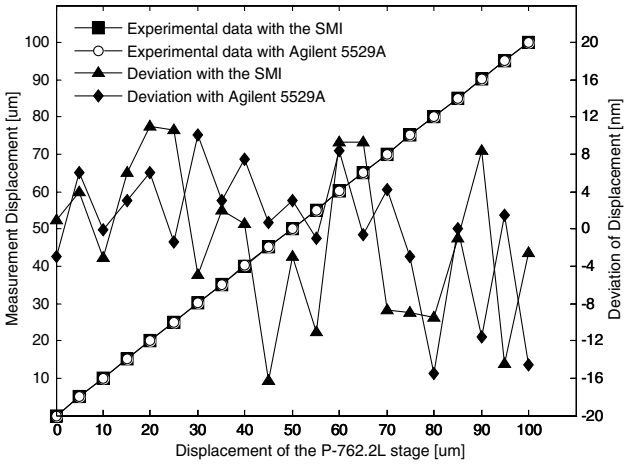

Fig. 6. Comparison of displacement measurements in the micrometer range.

5. Discussion

A. Resolution Analysis

From Eq. (2), and considering the limit of measurement accuracy influenced by sources of error, such as the variation of air refractive index, the laser source stability, and the accuracy in determination of the measured phase, the uncertainty of our system can be expressed as

$$\delta\Delta L = \sqrt{\left(\frac{\Delta L}{n}\delta n\right)^2 + \left(\frac{\Delta L}{\lambda_0}\delta\lambda\right)^2 + \left(\frac{\lambda_0}{4\pi n}\delta\Delta\varphi\right)^2}, \quad (5)$$

where ΔL is the measured displacement, δn is the uncertainty of air refractivity, $\delta\lambda$ denotes the uncertainty of a single wavelength, and $\delta\Delta\varphi$ is the accuracy in determination of the measured phase.

According to the updated Edlen equation, and neglecting the changes in air contents [20], when the environmental conditions deviate from the initial work state, the change of air refractivity can be expressed as

$$\Delta n_{tpf} = [0.00268(P - P_0) - 0.929(T - T_0) - 0.00042(f - f_0)] \times 10^{-6}, \quad (6)$$

where $P_0 = 101325$ Pa, $T_0 = 20°C$, and $f_0 = 1333$ Pa denote the air pressure, temperature, and humidity in the initial conditions of the measurement environment, respectively. P, T, and f represent the experimental conditions, which slightly deviate from the initial conditions. Because the measurement process is controlled in a short time (typically 2 s), the humidity and air pressure sensors show that there is no change in the ambient humidity and pressure of air in the laboratory. As a result, only a fluctuation within 1°C of the room temperature measured by the temperature sensor contributes to a change in the refractive index of air of $\delta n = 0.929 \times 10^{-6}$.

According to the parameters of the He–Ne laser engaged in the experiment, the center wavelength is 632.8 nm, and the short-term frequency stability is 1.5 ppm. Thus, the uncertainty of a single wavelength $\delta\lambda$ can be calculated as

$$\delta\lambda = \frac{\lambda_0^2}{c}\delta\nu \approx 0.9492 \times 10^{-6}\ \mu\text{m}. \quad (7)$$

Theoretically, the measured phase in our system can be established with almost arbitrary precision. However, it suffers from the high-frequency noise coming from the EOM electronics. Considering the

Table 2. Displacement Measurement Results in the Micrometer Range

System	Averaged Error (nm)	Standard Deviation (nm)	Maximum Error (nm)	Linearity Coefficient
The SMI	−1.0218	8.4009	16.3333	0.9984
Agilent 5529A	0.1210	6.9241	15.5000	0.9984

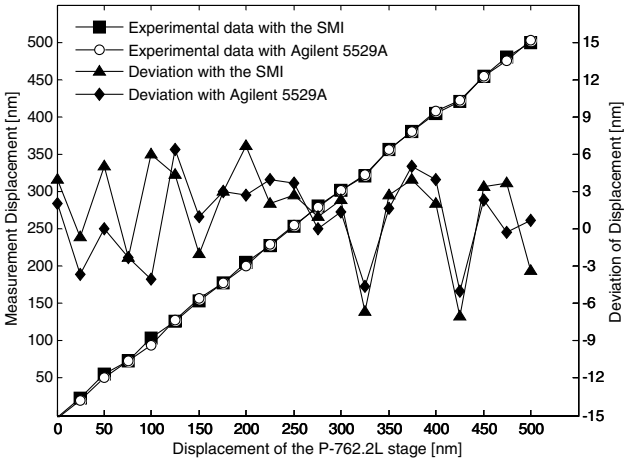

Fig. 7. Comparison of displacement measurements in the nanometer range.

deviations in the phase modulation depth excursion from the expected value, the ac component of the self-mixing interference signal can be written as

$$s(t) = mI_0 \cos\{\varphi(t) + [a + \delta_a(t)]\sin(w_m t + \beta)\}. \quad (8)$$

It is assumed that the deviation in the phase modulation depth is caused by Gaussian noise $\delta_a(t)$. Therefore, if the error-free displacement ΔL is subjected to such noise, the measured phase following the phase-determination algorithm can be rewritten as

$$\Delta\varphi_a = \frac{4\pi n \Delta L}{\lambda_0} + \delta_a \sin(w_m t + \beta), \quad (9)$$

where $\Delta\varphi_a$ is the measured phase subject to noises. As a result, the difference between the error-free phase and the calculated phase can be given as

$$\delta\Delta\varphi = \Delta\varphi_a - \Delta\varphi = \Delta\varphi_a - \frac{4\pi n \Delta L}{\lambda_0}$$
$$= \delta_a \sin(w_m t + \beta) \le |\delta_a|. \quad (10)$$

From the above equation, we can see that the accuracy in the determination of the measured phase induced by the modulation depth uncertainty is only related to the noise floor of the EOM electronics and is independent of the measured displacement. The smaller the noise $\delta_a(t)$ is, the smaller the phase noise influence on our system. We have examined the performance of EOM electronics, and an accuracy $\delta_a = 0.0132$ rad can be experimentally achieved.

Substituting these uncertainties into Eq. (5), we can get that $\delta\Delta L < 0.687$ nm when the measured displacement ΔL is less than 100 μm. If the measurement range is enlarged for 100 mm, $\delta\Delta L < 176.439$ nm can be obtained. These results show that the sinusoidal phase-modulating SMI can achieve subnanometer resolution in the micrometer range. The resolution of our system in the large range is currently limited by the uncertainty of a single wavelength of the laser. We believe that the resolution of our system can be further improved by using a laser source with a better frequency stabilization technique.

B. Multiple Feedback Effect Analysis

The principle of sinusoidal phase-modulating SMI is based on the consideration of only one instance of feedback from the external cavity. When the multiple reflection within the external cavity cannot be completely neglected, the intensity of the laser can be written as [21]

$$I = I_0\left[1 + m\cos(\phi)\sum_{j=0}^{\infty}(-\eta)^j\cos(j\phi)\right], \quad (11)$$

where η signifies the coupling effect from the external cavity back into the laser cavity, and the additional term in Eq. (11) (i.e., $j = 1, 2, \ldots$) is introduced by the multiple feedback light. As the running state of the interferometer is restricted within a weak feedback regime, the multiple feedback effect is small. So only the fourth lowest item of feedback is considered, and the simulated results of standard deviation in displacement reconstruction versus the fringe visibility m are shown in Fig. 9. We can find that the standard deviation in displacement measurement increases proportionally to the continuous increment of the fringe visibility. We attribute this error to the slight distortion of cosine function of the interference signal. Moreover, when the fringe visibility m is less than 0.2, this deviation does not increase significantly even if higher order feedback

Table 3. Displacement Measurement Results in the Nanometer Range

System	Averaged Error (nm)	Standard Deviation (nm)	Maximum Error (nm)	Linearity Coefficient
The SMI	1.4603	3.7954	7.00	0.9965
Agilent 5529A	0.8413	3.2329	6.3333	0.9884

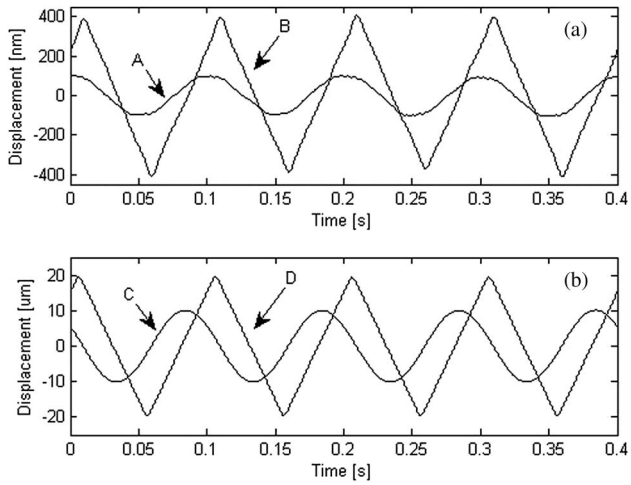

Fig. 8. Measurement results for displacement amplitude of about (a) 100 nm (curve A) and 400 nm (curve B) and (b) 10 μm (curve C) and 20 μm (curve D).

Table 4. Displacement Amplitude Measured by Our System and the Agilent 5529A Interferometer

	Curve A (nm)	Curve B (nm)	Curve C (nm)	Curve D (nm)
The SMI	106	397	10,128	20,213
Agilent 5529A	102	403	10,141	20,232
Difference	4	6	13	19

is included. As a result, it is possible to reduce this error at the cost of a detected SMI signal with low fringe visibility. The standard deviation is about 0.636 nm if $m = 0.1$, and the standard deviation is about 0.064 nm if $m = 0.01$.

C. Noises in Displacement Measurement

To test the noise level of our system, the stage was held stationary ($\Delta L = 0$) with an external cavity length of 20 cm. In this situation, the contributions of the measured displacement are only noises. The measurement result is obtained and shown in Fig. 10.

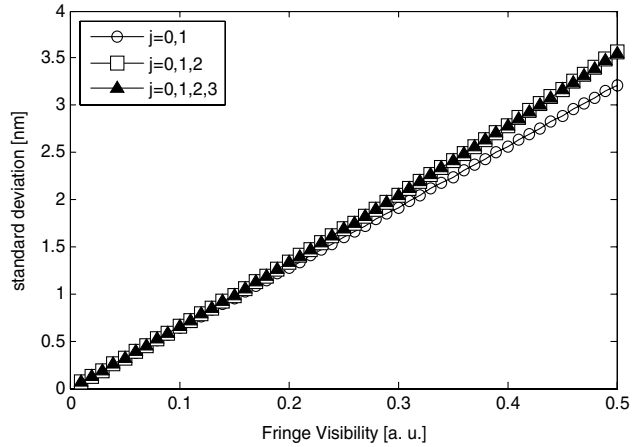

Fig. 9. Standard deviation of displacement measurement versus fringe visibility.

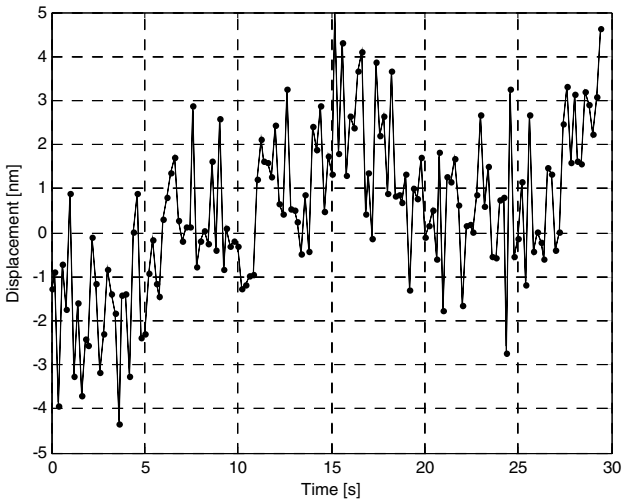

Fig. 10. Noises in the displacement measurement.

The high-frequency noise is mainly caused by fluctuation of the optical frequency and the performance of electronic devices, and the low-frequency noises come from the variation of air refractivity. The measurement result shows that the magnitudes of the noises are about 5 nm, with a root mean square value of 1.8066 nm during a 30 s period.

6. Conclusions

In this paper, we have developed and experimentally demonstrated a sinusoidal phase-modulating SMI for large displacement measurement. The measurement principle and the signal processing component of the interferometer were described in detail. The performance of the developed interferometer is evaluated through displacement measurement in the nanometer, micrometer, and millimeter ranges. Experimental results show that our system can be applied to large displacement measurement with nanometer accuracy. Furthermore, the sources of error that influenced the measurement resolution were analyzed, and the multiple feedback effect was discussed and evaluated as well. These results show that the development of the interferometer is useful for monitoring the displacement and vibration of the precision stage in a wide variety of research applications.

This work was supported by the National Natural Science Foundation of China (Grant Nos. 91123015, 61178044), the Specialized Research Fund for the Doctoral Program of Higher Education (20113207110004), the Natural Science Foundation of the Jiangsu Higher Education Institutions of China (Grant No. 11KJB510006), and the Science and Technology Innovation Fund for Graduates of Jiangsu Province Higher Education (Grant No. CX10B_400Z).

References

1. H. N. Hansen, K. Carneiro, H. Haitjema, and L. De Chiffre, "Dimensional micro and nano metrology," CIRP Ann. **55**, 721–743 (2006).

2. H. Martinussen, A. Aksnes, and H. E. Engan, "Wide frequency range measurements of absolute phase and amplitude of vibrations in micro- and nanostructures by optical interferometry," Opt. Express **15**, 11370–11384 (2007).
3. L. Chassagne, M. Wakim, S. Xu, S. Topçu, P. Ruaux, P. Juncar, and Y. Alayli, "A 2D nano-positioning system with sub-nanometric repeatability over the millimetre displacement range," Meas. Sci. Technol. **18**, 3267–3272 (2007).
4. B. Bodermann, E. Bhur, G. Ehret, F. Scholze, and M. Wurm, "Optical metrology of micro- and nanostructures at PTB: status and future developments," Proc. SPIE **7155**, 71550V (2008).
5. C. D. Frank, "High-resolution, high-speed, low data age uncertainty, heterodyne displacement measuring interferometer electronics," Meas. Sci. Technol. **9**, 1024–1030 (1998).
6. L. Xinqun, W. Clegg, D. F. L. Jenkins, and L. Bo, "Polarization interferometer for measuring small displacement," IEEE Trans. Instrum. Meas. **50**, 868–871 (2001).
7. K. Falaggis, D. P. Towers, and C. E. Towers, "Multiwavelength interferometry: extended range metrology," Opt. Lett. **34**, 950–952 (2009).
8. K. Falaggis and C. E. Towers, "Absolute metrology by phase and frequency modulation for multiwavelength interferometry," Opt. Lett. **36**, 2928–2930 (2011).
9. M. Suematsu and M. Takeda, "Wavelength-shift interferometry for distance measurements using the Fourier transform technique for fringe analysis," Appl. Opt. **30**, 4046–4055 (1991).
10. G. Guido, M. Norgia, S. Donati, and T. Bosch, "Laser diode self-mixing technique for sensing applications," J. Opt. A **4**, S283–S294 (2002).
11. G. Guido, B.-P. Simone, and D. Silvano, "Self-mixing laser diode vibrometer," Meas. Sci. Technol. **14**, 24–32 (2003).
12. U. Zabit, O. D. Bernal, T. Bosch, and F. Bony, "MEMS accelerometer embedded in a self-mixing displacement sensor for parasitic vibration compensation," Opt. Lett. **36**, 612–614 (2011).
13. P. de Groot, "Design of error-compensating algorithms for sinusoidal phase shifting interferometry," Appl. Opt. **48**, 6788–6796 (2009).
14. D. Guo, M. Wang, and S. Tan, "Self-mixing interferometer based on sinusoidal phase modulating technique," Opt. Express **13**, 1537–1543 (2005).
15. O. Sasaki and H. Okazaki, "Sinusoidal phase modulating interferometry for surface profile measurement," Appl. Opt. **25**, 3137–3140 (1986).
16. T. Suzuki, M. Matsuda, O. Sasaki, and T. Maruyama, "Laser-diode interferometer with a photothermal modulation," Appl. Opt. **38**, 7069–7075 (1999).
17. X. Wang, X. Wang, F. Qian, G. Chen, G. Chen, and Z. Fang, "Photothermal modulation of laser diode wavelength: application to sinusoidal phase-modulating interferometer for displacement measurements," Opt. Laser Technol. **31**, 559–564 (1999).
18. N. Servagent, T. Bosch, and M. Lescure, "Design of a phase-shifting optical feedback interferometer using an electrooptic modulator," IEEE J. Sel. Top. Quantum Electron. **6**, 798–802 (2000).
19. D. Guo and M. Wang, "Self-mixing interferometer based on temporal-carrier phase-shifting technique for micro-displacement reconstruction," Opt. Commun. **263**, 91–97 (2006).
20. K. P. Birch and M. J. Downs, "An updated Edlén equation for the refractive index of air," Metrologia **30**, 155–162 (1993).
21. B. Ovryn and J. H. Andrews, "Phase-shifted laser feedback interferometry," Opt. Lett. **23**, 1078–1080 (1998).